Wiley Analytical Science

Specific Heat Capacity Determination by DSC

April 19, 10:00am - 11:00am EDT

Specific heat capacity (cp) is an important, temperature-dependent material property and is often specified in material data sheets. It is a key property for improving technical processes such as injection molding, spray drying, or crystallization, as well as for the safety analysis of chemical processes and the design of chemical reactors.

Watch this session during the WAS Virtual Conference:

Dr. Jürgen Schawe

Register Now

This talk is sponsored by METTLER TOLEDO

ADVANCED FUNCTIONAL MATERIALS
www.afm-journal.de

A Universal Interfacial Strategy Enabling Ultra-Robust Gel Hybrids for Extreme Epidermal Bio-Monitoring

Zibi Wang, Ding Wang, Dong Liu, Xiang Han, Xiaoxu Liu, Hamdi Torun, Zhanhu Guo, Sidi Duan, Ximin He, Xuehua Zhang, Ben Bin Xu,* and Fei Chen**

A seamless and tough interface to integrate incompatible/immiscible soft materials is highly desired for flexible/wearable electronics and many soft devices with multi-layer structures. Here, a surfactant-mediated interfacial chemistry is introduced to achieve seamless and tough interfaces in soft multi-layer structures, with an ultra-high interfacial toughness up to ≈1300 J m^{-2} for the architectural gel hybrid (AGH). The reversible noncovalent interfacial interactions efficiently dissipate energy at the interface, thereby providing excellent durability. The interfacial toughness only decreases by ≈6.9% after 10 000 tensile cycles. This strategy can be universally applied to hybrid systems with various interfaces between an interior hydrogel (PAA, PVA, PAAm, and gelatin) and an exterior hydrophobic soft matter (ionogel, lipogel and elastomer). The AGH-based mechano-sensor presents high robustness and stability in a wide range of conditions, including open air, underwater, and various solvents and temperatures. Epidermal bio-monitoring, tactile trajectory, and facial expression recognition are demonstrated using the AGH sensors in various environments. A rich set of electrophysiological signals of high quality are acquired.

1. Introduction

Complementary bio-structure with hydrophobic and hydrophilic components exists in nature to fulfill the fundamental functions in various length scales.[1,2] Amphipathic lipid molecules forming cell membranes are examples at cellular level to ensure the metabolism.[3,4] Whereas, mammalian skin integrating with the complementary units (oily hydrophobic epidermis and water-contained dermis) to facilitate the desired physiological function is another example at a macro level.[5–7] Inspired by these bio-structures, hybrid integration of hydrogels with other incompatible/immiscible soft materials, including elastomer, lipid gel (lipogel) and ionic liquid gel (ionogel) is a promising strategy to realize multi-functions in a variety of applications, including responsive materials,[8–10] soft electronics,[11–13] biomedical lubrication[14,15] and flexible actuators.[16,17] However, the weak interface caused by the intrinsic incompatibility between hydrogel and other soft materials (interfacial toughness < ≈1 J m^{-2}),[18–20] has severely hindered the practical implementation of concept.

Effective bonding strategies between hydrogels and other soft materials has been extensively researched.[20–25] Covalently anchoring long-chain hydrogel networks on solid substrates has secured an interface with a toughness comparable to tendon and bone tissues of human (≈800 J m^{-2}).[22,26] Another method to construct an interfacial interpenetration structure, is to utilize hydrophobic and hydrophilic initiators to form a hydrogel layer on the elastomer surface.[27,28] These reported strategies mainly focus on creating a hydrogel coating upon hydrophobic soft materials.[29] On the other hand, the reciprocal strategy of controllably generating a hydrophobic layer on the hydrogel surface has not been well explored.

The hybrid structure of coating a hydrophobic layer on the hydrophilic hydrogel surface can be paramount to realize soft matter-based epidermal bio-electronics, with predominating potential applications in personal bio-monitoring[12,30] and healthcare.[31,32] These devices usually consist of an external dielectric layer to hinder the mass exchange[33,34] and internal layer to create desired conductivity and responsiveness.[35] Suo et al.[36] reported to graft an elastomer layer on hydrogel surface to initialize a tough interface. Despite the functionality,

Z. Wang, D. Liu, X. Han, X. Liu, F. Chen
School of Chemical Engineering and Technology
Xi'an Jiaotong University
No. 28, Xianning West Road, Xi'an, Shaanxi 710049, China
E-mail: feichen@xjtu.edu.cn

D. Wang, H. Torun, Z. Guo, B. B. Xu
Mechanical and Construction Engineering, Faculty of Engineering and Environment
Northumbria University
Newcastle upon Tyne NE1 8ST, UK
E-mail: ben.xu@northumbria.ac.uk

S. Duan, X. He
Department of Materials Science and Engineering
University of California, Los Angeles (UCLA)
Los Angeles, CA 90095, USA

X. Zhang
Department of Chemical and Materials Engineering
University of Alberta
Alberta T6G 1H9, Canada
E-mail: xuehua.zhang@ualberta.ca

The ORCID identification number(s) for the author(s) of this article can be found under https://doi.org/10.1002/adfm.202301117.

DOI: 10.1002/adfm.202301117

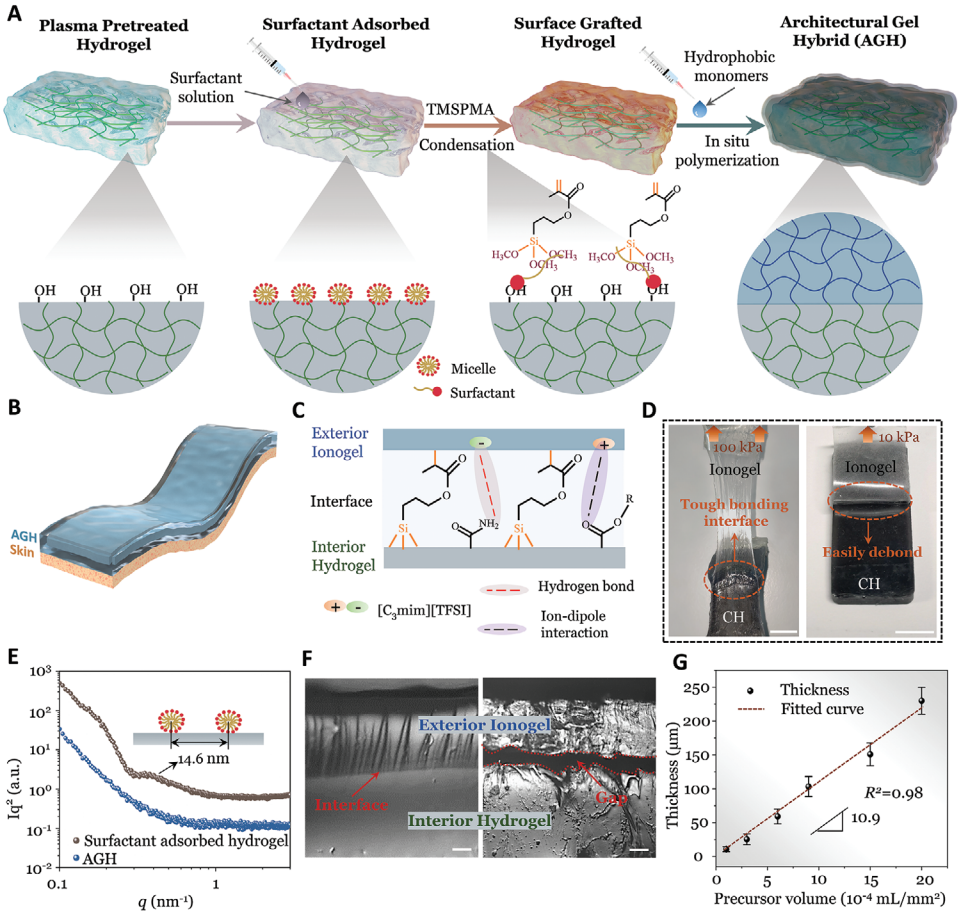

Figure 1. The SMIC enabled interfacial strategy for architectural gel hybrid (AGH). A) Illustration of SMIC strategy. B) Schematic of conformability of AGH. C) Illustration diagram of the molecular interactions at AGH interface. D) Snapshots of hand peeling test for AGH (left) and CH/Ionogel without SMIC (right). Scale bar: 1 cm. E) SAXS spectra of surfactant adsorbed hydrogel and AGH. F) Microscopic observations of the interface for AGH (left) and CH/Ionogel without SMIC (right). Scale bar: 20 μm. G) The thickness of exterior ionogel as a function of precursor volume.

this approach may considerably sacrifice the homogeneity of both layers, due to the pre-incorporation of coupling agents. Recently, our group developed structural gel composites for a robust interface strategy by forming a lipogel coating out of the hydrogel core.[29] However, the method works only on the hydrogel surfaces with specific functional groups. Therefore, a universal strategy that can controllably construct a hydrophobic soft material coating on various hydrogel surfaces to create tough and durable interfaces is still highly desired.

Herein, we propose an interfacial strategy based on surfactant-mediated interfacial chemistry (SMIC, **Figure 1**A) to controllably form a hydrophobic soft layer seamlessly on a hydrogel surface without compromising the homogeneity of either phase. The adsorbed surfactant micelles anchor the hydrophobic silane agents on the hydrophilic hydrogel surface and host the polymerization subsequently. This interfacial strategy achieves a tough interface (up to ≈1300 J m^{-2} in interfacial toughness), unique solvent resistance, and remarkable durability (≈6.9% loss) after 10 000 stretching cycles. This SMIC approach works universally on the interfaces between various exterior soft materials (lipogel, ionogel and elastomer) and interior hydrogels. The exemplified architectural gel hybrid (AGH) can perform precise epidermal bio-monitoring at various environments (open air, different solvents and temperatures).

2. Results and Discussion

2.1. The Realization of SMIC Enabled Interfacial Strategy

The SMIC interface strategy is illustrated in Figure 1A, with an exemplified fabrication of an AGH, to generate a hydrophobic ionogel layer on a conductive hydrogel (CH) surface (Figures S1–S4, Methods).[22] The adsorbed surfactant sodium dodecyl sulfate (SDS) micelle plays a key role to overcome the incompatibility between a hydrophobic silane coupling agent (methoxy groups) and the hydrophilic CH surface (hydroxyl groups) by bridging two phases (Figure 1A; Figure S5, Supporting Information). The surrounding hydrophobic reaction atmosphere (ethyl acetate solvent) ensured a uniform distribution of coupling agent only on the CH surfaces (Figure S6, Supporting Information). The FTIR results show new peaks at 3013 and 1677 cm^{-1} (corresponding to vinyl groups), 2923 and 2854 cm^{-1} (corresponding to the packing of alkyl chains in

surfactants molecules), and 806 and 1084 cm^{-1} (corresponding to Si—O), which confirm the successful introduction of vinyl groups on the CH by the condensation reaction between the silane coupling agent, 3-(trimethoxysilyl) propyl methacrylate (TMSPMA), and –OH (Figure S7, Supporting Information).

The soft hydrophobic gel layer (ionogel) is synthesized by copolymerizing the vinyl groups on CH surfaces with hydrophobic monomers and a fluorinated ionic liquid (IL) 1-Propyl-3-methylimidazolium bis(trifluoromethylsulfonyl)imide ([C_3mim][TFSI]) (Figures S8–S11, Supporting Information). The IL offers the noncovalent interactions of interface. As such, a synergy of covalent bond and noncovalent interactions (hydrogen bonds and ion-dipole interactions) is expected to occur on the interface (Figure 1C and Figure S12, Supporting Information).[37] The FTIR spectra in Figure S13a (Supporting Information), verifies the covalent bonds between the ionogel and CH, with the disappearance of vinyl groups peaks and appearance of new peaks at 1176 cm^{-1} (CF_3) and 1031 cm^{-1} (S-N-S). Meanwhile, the characteristic peaks of S-N-S and CF_3 in [TFSI]$^-$, and imidazolium ring in [C_3mim]$^+$ display a slight shift, due to the hydrogen bonds and ion-dipole interactions at interface (Figure S13b, Supporting Information).[38]

The robust interface of AGH is empirically assessed via a peeling test (Figure 1D; Movie S1, Supporting Information). The ionogel layer can be easily removed from the CH surface under a peeling force, for the CH/Ionogel hybrid without SMIC (Movie S2, Supporting Information). In order to trace the occurrence of SMIC, small-angle X-ray scattering (SAXS) measurements and dynamic light scattering (DLS) analysis are performed to observe the variation of micelle before and after the interface construction. The SDS solution exhibits a distinct single peak, indicating that the surfactants are distributed in the form of micelles with a diameter of ≈18.2 nm (Figure S14, Supporting Information). Prior to generating the ionogel layer, a single broad peak appears with a distribution of the micelles adjacent distance of ≈14.6 nm (Figure 1E).[39,40] For the AGH, the scattering peaks completely disappear, since the adsorbed micelle layer on hydrogel dissociates into small surfactant molecules to anchor the vinyl groups and subsequently initialize the polymerization of hydrophobic monomers (Figure 1A). A seamless and tightly bonded interface (Figure 1F) is observed under optical microscope between the hydrophilic CH and hydrophobic ionogel for AGH (Figure S15, Supporting Information). With SMIC, the thickness of external ionogel can be controlled as a function of the amount of precursor (Figure 1G; Figure S16, Supporting Information). In contrast, an explicit gap (≈30 µm in width) with irregular edge is observed for the CH/Ionogel hybrid without SMIC.

2.2. The Characterizations of Interface

To quantitatively characterize the AGH interface, a 90° peeling experiment is performed to measure the interfacial toughness (**Figure 2**A). As shown in Figure 2B and Figure S17 (Supporting Information), the AGH presents an interfacial toughness of 396 J m^{-2}, ≈300-fold higher than that of CH/Ionogel hybrid without TMSPMA (1.34 J m^{-2}) and an order of magnitude higher than that of CH/Ionogel hybrid without surfactant treatment (36 J m^{-2}). For the CH/Ionogel hybrid without IL, the interfacial toughness is reduced by 27.8%. Next, we change the reaction time between TMSPMA and –OH anchored on the CH surfaces while maintaining the concentration. As the reaction time rises, the interfacial toughness of AGH first increases and then remains constant, and the optimal interfacial toughness is achieved at a reaction time of 90 min (Figure 2C; Figure S18, Supporting Information). More SDS and prolonged reaction time lead to a rise in interfacial toughness by providing favorable reaction kinetics with a certain threshold (Figure 2D). However, excessive concentration of SDS or overlong reaction time degrades the interfacial toughness of AGH, because the formation of hydrogen bonds between the micelles and CH surfaces reduces the hydroxyl sites for reacting with silane coupling agents (Figure S19, Supporting Information). This SMIC strategy can even work on different types of surfactants, including anionic, cationic, amphiprotic, and nonionic surfactants (Figure 2E, Figures S20 and S21, Supporting Information).

We next study the role of noncovalent interactions on AGH interface by varying the IL concentration. As the IL concentration increases, the obtained interfacial toughness initially increases and then decreases (Figure 2F; Figure S22, Supporting Information). Further increase in IL reduces the toughness of the exterior ionogel (Figure S23, Supporting Information) due to the plasticization of IL, which is detrimental for the interfacial toughness.[22] The increase of interfacial toughness imparted by moderate IL is correlated to the following factors. First, the chemically stable fluorinated IL can provide a stable liquid environment for the in situ polymerization reaction on CH surface.[41] Second, the IL brings high mobility to polymer chains due to the plasticizing effect (Figure S9, Supporting Information),[42,43] which contributes to the adequate linkage of polymer chains at the interface between CH and ionogel through covalent interactions. Third, the IL can interact with CH surface by ion-dipole interactions and hydrogen bonds (Figure S12, Supporting Information).[37,38] Even though these noncovalent interactions are weaker than the covalent interactions, the reversible noncovalent bonds can dissipate the applied energy of interface region when the interface deforms, which will retard the fracture of covalent bonds and diminish the stress concentration of interface (Figure S24, Supporting Information).

Cyclic tensile tests are performed on the AGH for 10 000 times at 50% strain, to verify the dynamic noncovalent interactions (provided by IL) on interface (Figure S25, Supporting Information).[44] For the AGH with IL, the interfacial toughness decreases by 29% after 10 000 cycles, as the noncovalent interactions at interface break to dissipate the energy (Figure 2G; Figure S26a, Supporting Information). With the extension to 120 min in resting time, the interfacial toughness gradually recovers to 93.1% of the original value (92.2% during 60 min), due to the restoration of reversible noncovalent interactions (Figure S27a, Supporting Information). Such dynamic interactions at the interface is evidenced by the shift of imidazolium ring in [C_3mim]$^+$ and CF_3 peaks corresponding to hydrogen bonds and ion-dipole interactions, as well as the almost constant Si—O peak corresponding to covalent bond (Figure 2H). On the contrary, the interfacial toughness for AGH without IL

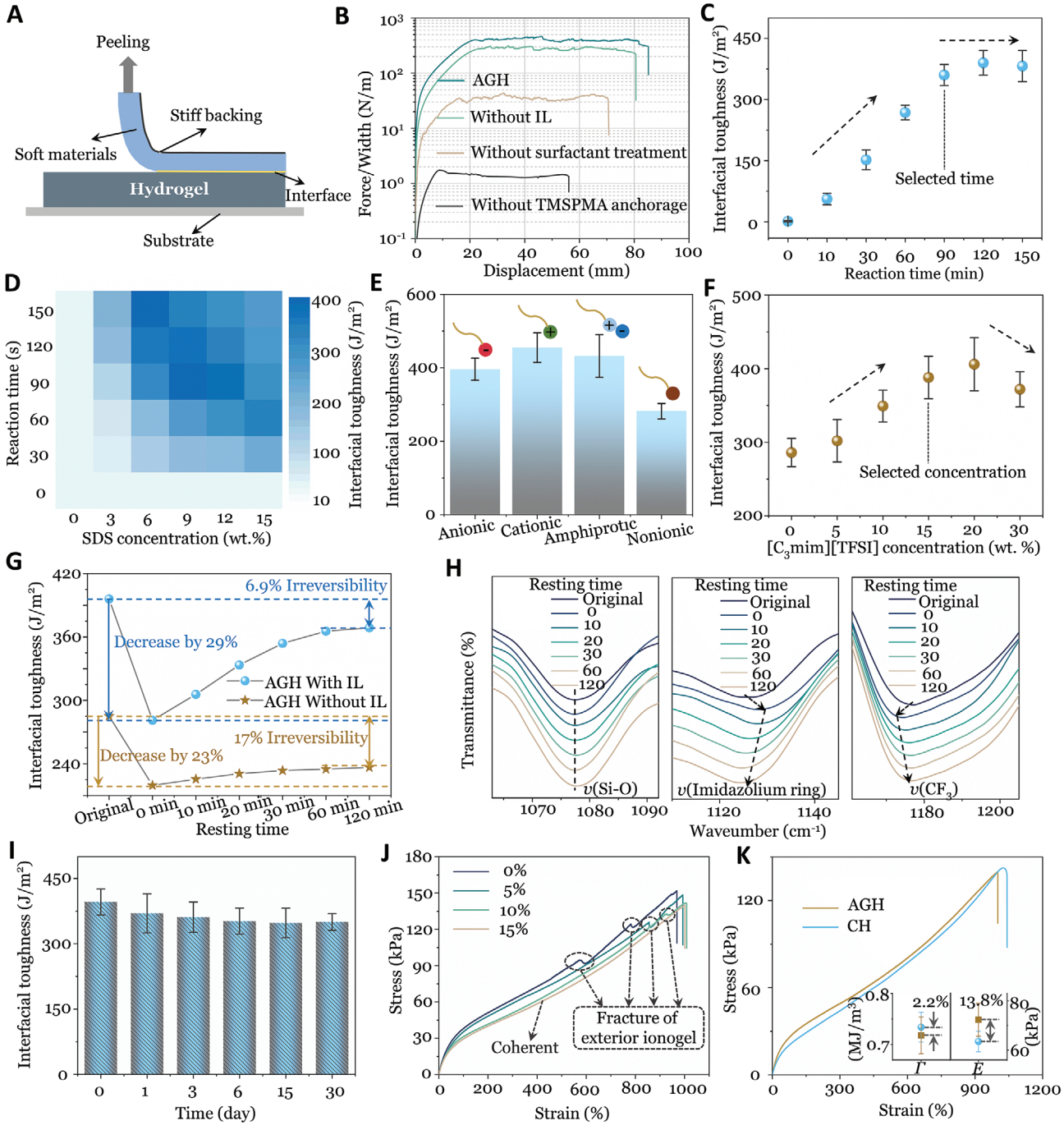

Figure 2. Mechanical and chemical characterizations of interface. A) Schematic illustration of 90° peeling test. B) Representative peeling force-displacement curves for AGH, CH/Ionogel composites without surfactant treatment/modification by TMSPMA/IL. Interfacial toughness of AGH with C) different reaction time, D) different SDS concentration and immersing time, E) different surfactants (the anionic refers to SDS, the cationic refers to CTAB, the amphiprotic refers to BS-12, the nonionic refers to Pluronic F127, page 3 in Supplementary information), F) various IL concentration, G) and without IL during different resting time after 10 000 stretching cycles. H) FTIR spectrum of AGH at original state, after stretching cycles and different resting time. I) Interfacial toughness of AGH during 30 days. J) Stress-strain curves of AGH with different IL concentrations. K) Comparison of stress-strain curves between CH and AGH, and corresponding toughness (Γ) and elastic modulus (E).

presents 17% irreversible reduction (Figure 2G; Figure S26b, Supporting Information), due to the partial sacrifice of irreversible covalent bonds of interface region (Figure S27b, Supporting Information).[45] Benefiting from the synergy of covalent bonds and noncovalent interactions, our AGH presents a long-term stability with a highly reliable interfacial toughness for 30 days (Figure 2I; Figure S28, Supporting Information). It is worth noting that the interfacial toughness presents a 11.1% reduction

at the first 6 days, due to the slight decrease in the toughness of AGH caused by a small amount of dehydration (Figure S29, Supporting Information). However, the interfacial toughness stabilizes from 6th day onward.

The tough interface and controllable exterior layer fulfil AGH with excellent mechanical robustness (Figure S30, Supporting Information). As shown in Figure 2J and Figure S31 (Supporting Information), the black circles represent the fracture of ionogel. It is found that the fractured strain and fractured toughness increase with the enhancement of IL. The stress-strain behaviors of AGH show similar elongation and toughness behaviors with that of CH, although the elastic modulus increases by 13.8% compared with CH (Figure 2K), due to the relative high modulus of ionogel (Figure S23, Supporting Information). This behavior depends on the action of the tough and stretchable interface, as well as on the adjustable mechanical properties of the double gels (Figures S23 and S32, Supporting Information).

2.3. The Universality of SMIC Based Interface and Unique Characteristics for AGH

The SMIC strategy can be extended to a variety of exterior soft materials (iongel, lipogel, elastomer) and interior hydrogels (PAAm-based, PAA-based, PVA-based, Gelatin-based hydrogel) (**Figure 3**A, Figures S33 and S34, Supporting Information). An interfacial toughness over 1300 J m^{-2} is achieved for the

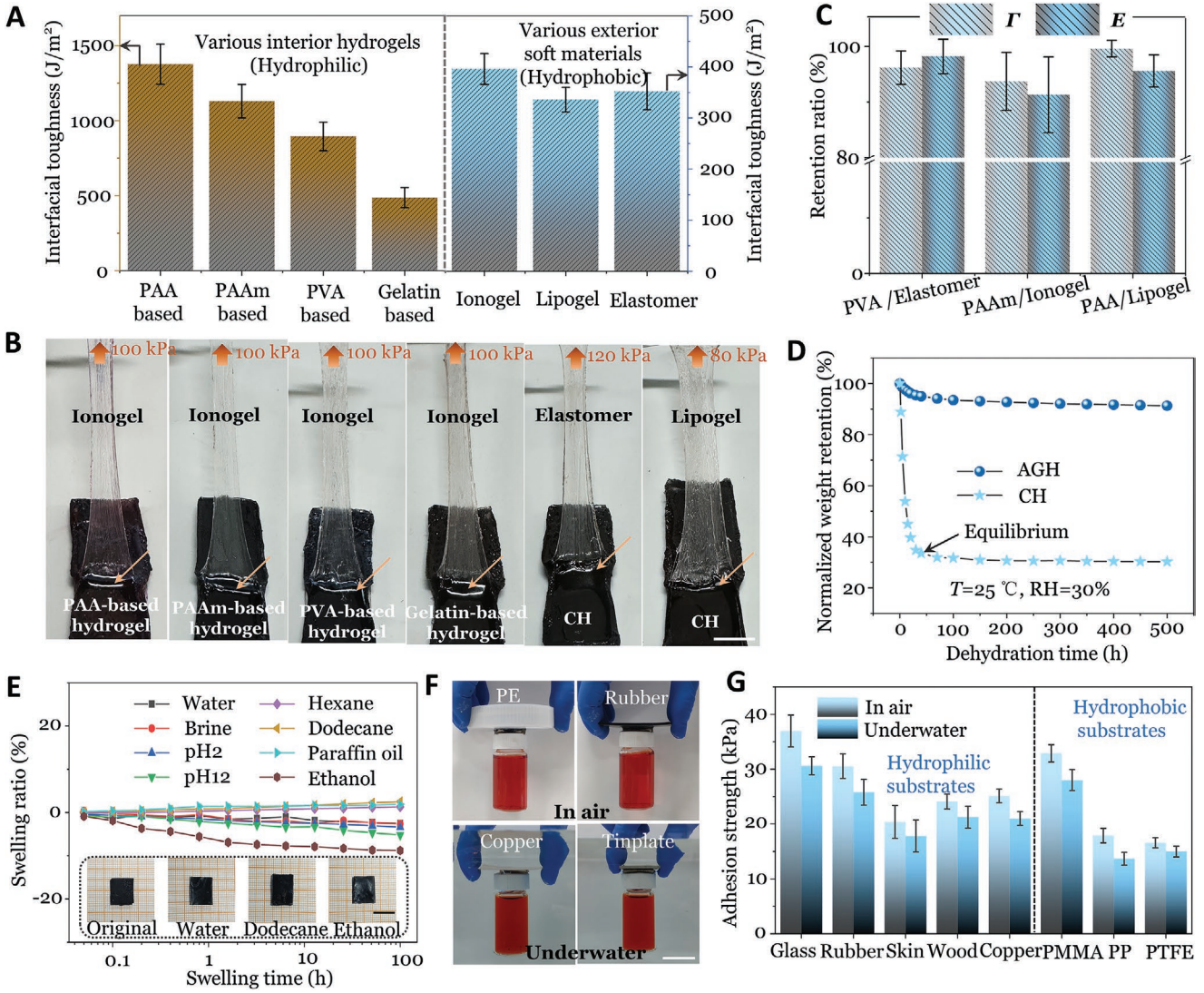

Figure 3. Universality of SMIC based interfacial strategy and other properties of AGH. A) Interfacial toughness of various types of interior hydrogels and exterior soft materials. B) Snapshots of AGH interface constructed by different combination of interior and exterior materials. Scale bar: 1 cm. Elastomer refers to P(BA-co-IBA), lipogel refers to P(BA-co-LA)/paraffin oil (page 6 in Supplementary information). C) Retention ratio of toughness (Γ) and elastic modulus (E) between different types of hydrogel and corresponding different AGH. PVA refers to PVA-Chitosan hydrogel, PAAm refers to PAAm-Alginate hydrogel, PAA refers to P(AA-AAm)-Fe^{3+} hydrogel (page 4,5 in Supplementary information). D) Weight variation of CH and AGH during 500 h. E) Swelling behavior of AGH in various solvents. Scale bar: 2 cm. F) Snapshots of surface adhesion of AGH to different substrates. Scale bar: 2 cm. G) Surface adhesion strength of AGH to different substrates in air and underwater.

Ionogel/P(AA-AAm)-Fe^{3+} hybrid system. When using other hydrophobic soft materials as the exterior layer, i.e. elastomer or lipogel, high interfacial toughness can be maintained with a value ranging from 320 to 396 J m^{-2} (Figure 3A; Figure S35, Supporting Information). The SMIC enabled robust interfaces between different hydrogels and soft materials are demonstrated in Figure 3B, with a peeling load (≈100 kPa) applied on the controllable thickness of exterior hydrophobic layer. All AGH show retained mechanical properties, consistent with the interior hydrogel (Figure 3C; Figure S36, Supporting Information).

The external hydrophobic layer enabled by SMIC can effectively protect the interior CH in AGH from swelling/de-swelling (Figures S37 and S38, Supporting Information). In Figure 3D, the AGH presents only 10% weight loss after 500 h at the open-air environment (25 °C and 30% relative humidity). On the contrary, the virgin CH reaches kinetic equilibrium and becomes stiff within 50 h. The obtained AGH presents remarkable stability in different solvent environments, i.e. polar solvents (e.g. water, brine, acid and alkaline solutions), nonpolar solvents (e.g. hexane, dodecane, paraffin oil) and even in ethanol during immersion of 100 h (<10%, Figure 3E; Figure S39, Supporting Information). Mechanical properties (<26% loss in stress and strain), the interfacial toughness (<42% loss) and internal microstructures can be reasonably maintained after immersion for 24 h (Figures S40–S42, Supporting Information). It is worth noting that the decline in the interfacial toughness and mechanical properties is due to that the chain relaxation after immersion in solvents brings a reconfiguration of polymer chains and minor solvents exchange with ionogel.[29,46] This unique anti-swelling feature attributes to that the exterior ionogel containing inert fluorine-containing molecules can lower surface free energy (Figure S43, Supporting Information), and serve as a barrier to suppress the diffusion of external small molecules into the core CH (Figure S44, Supporting Information).

Surface adhesion is crucial for wearable mechanoreceptor to construct epidermal human-machine interface. The AGH possesses strong surface adhesion to different substrates both in air and underwater (Figure 3F; Figure S45, Supporting Information), as the IL in AGH can form dipole-dipole or ion-dipole interactions with substrates (Figure S46, Supporting Information). The adhesions are over 13 kPa to different substrates both in air and underwater (Figure 3G; Figure S45, Supporting Information), including hydrophilic substrates (e.g. glass, rubber, porcine skin, wood, copper) and hydrophobic substrates (PMMA, PP, PTFE). Moreover, the AGH obtained by SMIC can also maintain the intrinsic chemical and physical feature of hydrogel (Figures S47 and S48, Supporting Information).

2.4. The Mechano-Sensing Feature of AGH

The mechano-sensitivity of AGH in **Figure 4**A and Figure S49 (Supporting Information) shows a high sensitivity in a broad strain range, with a *GF* of 14.43 during 500–1000% strain. Here the gauge factor (*GF*) is defined as $GF = (\Delta R/R_0)/\varepsilon$.[47] The high sensitivity is attributed to the robust interface with a high-fidelity transfer of stress to the internal CH. Accurate and reliable electrical signals are generated at low strains (0.5–5%), high deformations (50–500%) and various frequencies (0.08–0.64 Hz) with a fast response (156 ms, Figure S50, Supporting Information). As a comparison, the CH/Ionogel composite without SMIC produces irregular variation in electrical signals when stretching over 50% strain (Figure S51, Supporting Information), due to the interfacial slippage/failure between CH and ionogel. A remarkable reproducibility of stable signals is presented from the long-term sensing durability test of AGH by cyclic stretching to 10% strain over 2000 times (Figure 4B). The CH/Ionogel without SMIC generates irregular and dissimilar output signals (Figure 4C). The AGH also demonstrates outstanding durability in different solvent environments (Figure 4D; Figure S52, Supporting Information). In comparison to the works previous reported, our AGH demonstrates superior overall performance (Table S1, Supporting Information). These results have inspired us to explore the practical application as a mechano-sensor.

The AGH sensor can be utilized to monitor human health and motions when being attached to the human skin (Figure S53 and Movie S3, Supporting Information). In a demonstration, the AGH sensor can distinguish and monitor movements of a knee by producing specific electrical signals at large deformations (Figure 4E). When attaching to the wrist (Figure 4F), the AGH sensor can detect subtle pulse vibrations (small deformation scenario) with distinct three specific waves of percussion (*P*), tidal (*T*) and dicrotic (*D*) in air and underwater. These signals provide valuable data for personal healthcare monitoring and management.[48,49] The AGH sensor can also detect the pulse underwater with either low (0 °C) or high (50 °C) temperature, by showing pulse readings of 76–78 beats/min with <2.7 % standard deviation (Figure 4G). Moreover, our AGH sensor can transduce the reliable specific signals in response to multi-mode motions, i.e. finger bending/stretching (Figure 4H)/pressing (Figure S54, Supporting Information) in different liquid environments.

2.5. Demonstration of Tactile Trajectory Tracking and Epidermal Bio-Physiological Signal Acquiring

A tactile trajectory-tracking system is constructed by sandwiching 25 pixels array (5 × 5 AGH sensing patch units) with VHB substrate and PET film cover layer, where the silver wires are utilized to connect the sensing units (**Figure 5**A; Figure S55, Supporting Information). When a finger gradually moves on the sensing plate, the AGH unit can transmit the mechanical signals caused by the tactile trajectory to the internal CH for the generation of specific electrical signals in real time (Figure 5B). Accompanying with the output signals distribution related with the stress intensity (Figure 5C), the spatial tactile trajectory can be reconstructed in real time.

We also assemble and deploy an AGH sensing system on human face to detect the dynamic deformation of facial muscles. The signals will be fed back to the electronic system and realized in the computer-generated imagery (CGI), which is pivotal for science fiction movie shooting, human-machine interfaces, and personal health management. By applying the bionics principle, an array of ten AGH sensor are placed symmetrically on the volunteer's face (Figure 5D). When the male

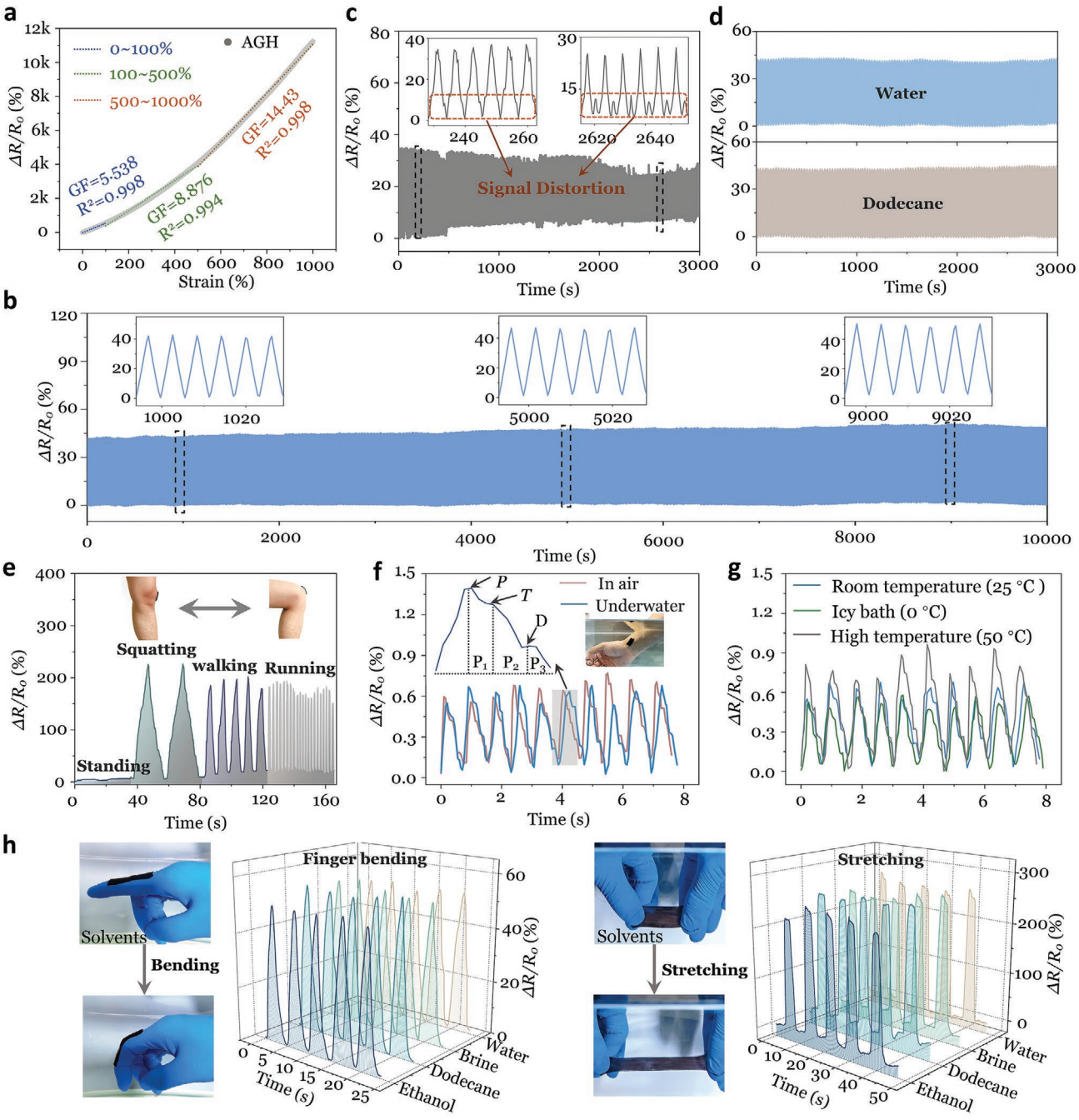

Figure 4. The AGH based mechano-sensing. A) Gauge factor (GF) of AGH sensor. Response to 10% strain by stretching B) AGH based sensor for 2000 cycles and C) CH/Ionogel composite without SMIC for 600 cycles. D) Response to 10% strain by stretching AGH for 600 cycles in both water and dodecane solvents. The detection of AGH sensor to E) human motions and F) pulse vibration. G) Response curves of pulse vibration at different underwater temperatures. H) Snapshots and output signals of AGH sensor to finger bending and stretching in various solvents.

volunteer expresses emotions, i.e., smile, frustrate and surprise (Figure 5E), AGH sensor array produces distinct signal patterns by capturing the dynamic muscle deformations in multi-locations (Figure 5F). By feeding the signal into the preset algorithm, we re-construct the signals into an avatar to respond to the corresponding expression. As it can be seen in Figure 5E, each emotion can be recorded by the avatar in real time (Movie S4, Supporting Information), based on the dedicated output signals decoding each facial expression (Figure 5F; Figure S56, Supporting Information). Same effectiveness of avatar has been found on female volunteer (Figure 5G; Figure S57 and Movie S5, Supporting Information).

To demonstrate the stability and anti-swelling capability of AGH, we further monitor the dynamic facial expressions

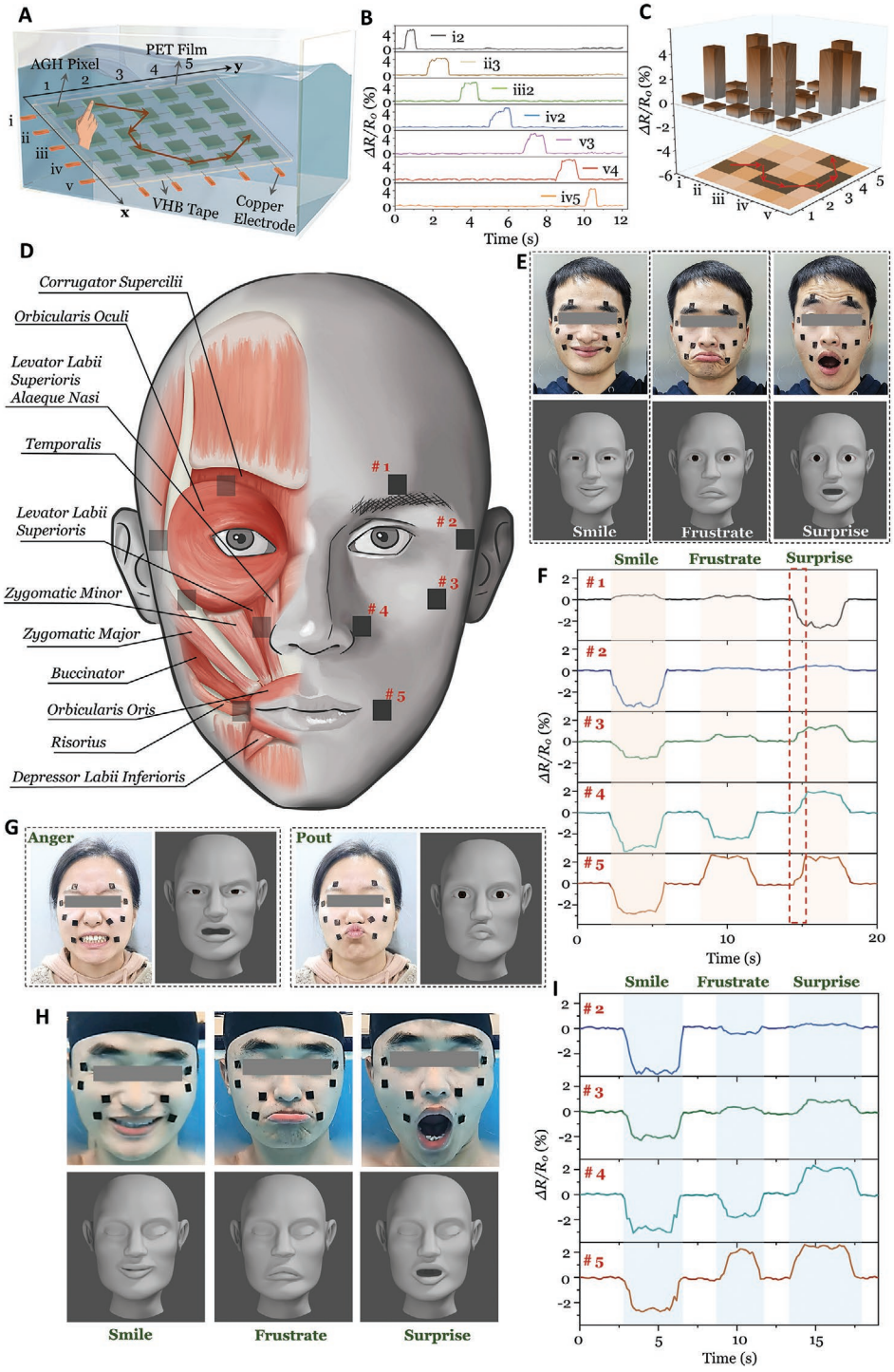

Figure 5. Tactile trajectory and avatar to reflect dynamic bio-physiological signal acquiring in real time. A) Schematic diagram of 5 × 5 AGH sensing units and the finger movement trajectory underwater. B) Outputted electrical signals according to the trajectory. C) Corresponding $\Delta R/R_0$ magnitudes. D) The schematic analysis on facial muscles that determine the expression and deployment of sensors on human face. E) Different expressions on a male volunteer's face and the corresponding avatars. F) Corresponding sensing signals and detailed expression variations for (E). G) Snapshots of expressions on a female volunteer's face and corresponding avatars. H) Snapshots of expressions on the male volunteer's face underwater and the corresponding avatars. I) Outputted signal curves corresponding to these male expressions underwater.

in underwater scenario. In Figure 5H, series of output signal waveforms are recorded in response to each facial expression (Figure 5I), which is in consistence with those in air. It should be noted that there is a fluctuation of signal curves, due to the influence of water waves. However, these disturbances do not affect the accurate and precise reflection of expressions

(Figure 5H; Movie S6, Supporting Information). Therefore, we believe this AGH sensor system open a new avenue for barrier-free underwater communication with digital avatar.

3. Conclusion

In this work, we develop a novel SMIC strategy to generate a robust interface, to construct a layer of hydrophobic soft material on hydrogel. The SMIC fulfils a robust interface between interior hydrogel and exterior soft material without altering their internal structures. With the synergistic effect of covalent linkage and non-covalent interactions, the demonstrated interface exhibits excellent long-term durability and fulfils the anti-swelling characteristics to the architectural gel hybrid. As a versatile strategy to design robust interface, it can be applied to a combination of various types of interior hydrogels and exterior hydrophobic soft materials. By uniformly encapsulating the interior hydrogel, we have ensured that the resulting structure maintains a relatively high level of stability even when exposed to different solvents and environments. The reported strategy for achieving robust and durable interface enables plentiful applications that require long-term deformation and robust mechano-sensing performance in challenging scenarios (under water, in organic solvents. varied temperatures, etc.). A wide range of applications have been demonstrated with epidermal sensor, dynamic tactile trajectory tracking and facial expressions recognition with digital avatar in real time.

4. Experimental Section

Preparation of Interior Hydrogel: Taking the conductive hydrogel (CH) P(AAm-*co*-HEA)/MXene as an example. AAm (5 g), HEA (1 mL), and MXene aqueous solution (concentration of 5.2 wt.‰, 3.9 mL) were added into DI water (16 mL) and stirred for 30 min. Subsequently, APS (35 mg) was dissolved in above mixture under stirring, following by removing O_2 from the solution for 10 min with N_2. Finally, the obtained mixed solution was transferred to a homemade glass mold (50 mm × 20 mm × 10 mm), and placed in 60 °C environment for 2 h to form CH. The obtained CH was defined as CH-*x*%, where *x*% is the mass fraction of MXene (Table S2, Supporting Information). If not specified, the CH refers to the CH-15%. Additionally, the synthesis of other interior hydrogels is shown in Supplementary information.

Surface Grafting of Hydrogel: The purpose of surface grafting is to introduce vinyl groups on the surfaces. Before introducing vinyl groups, the prepared CH was first treated by oxygen plasma for 3 min to ensure the sufficient –OH on hydrogel surface, followed by immersing in a certain concentration of SDS surfactant solution for 90 s. The SDS micelles were mainly adsorbed on the CH surface layer, due to that the limited immersing time went against permeating far into CH. Then, a certain amount of DI water was added to TMSPMA (4 mL) to partially hydrolyze the methoxy terminal groups and generate the Si—OH for postreaction. After that, the hydrolyzed TMSPMA was dispersed in ethyl acetate (20 mL) with the aid of ultrasonic treatment, because the TMSPMA was more likely to disperse in ethyl acetate than water. During the process, the remaining moisture was removed due to the stratification of water and ethyl acetate. Finally, the above CH was immersed into the solution and incubate for 90 min at room temperature. In this process, vinyl groups could be bonded on the surface of hydrogel with the aid of surfactant due to the condensation between hydrolyzed TMSPMA and the –OH on CH. After the reaction ended, the hydrogel was put out, rinsed with water and dried for 3 min under N_2 flow.

Preparation of Architectural Gel Hybrid (AGH): The AGH was synthesized through in situ polymerization with vinyl groups on the surface of grafted hydrogel by one-step photopolymerization. Taking the ionogel exterior layer as an example, TFEA (2 mL), MEA (2 mL), [C_3mim][TFSI] ionic liquids with various concentrations, and photoinitiator (2-hydroxy-2-methylpropiophenone, 20 µL) were evenly mixed to form ionogel precursor solution with the aid of ultrasonic treatment (Table S3, Supporting Information). Subsequently, the previous surface grafted hydrogel by TMSPMA was placed on a quartz glass and immobilized with a square rubber mould. The rubber mould was slightly higher than hydrogel for providing the spaces of subsequent polymerization of ionogel, where the thickness of the outer ionogel layer could be controlled by adjusting the height of rubber mold. Finally, a certain amount of ionogel precursor solution was added to the surface of hydrogel and exposed to UV irradiation for 30 min to construct ionogl layer. The same operation for other 5 surfaces of hydrogel was applied. In this experiment, if not being specified, the AGH refers to the interior hydrogel of CH containing 15% MXene and the exterior ionogel containing 15% IL. Additionally, the preparation of other diverse exterior soft layers on the surface of hydrogel are similar with the ionogel and shown in Supplementary information in detail.

Fabrication of AGH Based Mechano-Sensor: First, the conductive hydrogel (CH) grafted with TMSPMA was placed on a transparent quartz glass and fixed with rubber mold. Second, two silver wires with diameter of 0.1 mm and coated with paraffin at one end were embedded in the ends of the CH respectively. Subsequently, the precursor used for synthesizing the exterior layer (ionogel) was dripped on the surface of CH and covered with a quartz glass. UV irradiation was performed for 30 min to polymerize the precursor and form ionogel on the surface of CH. During the process of polymerization, the two silver wires were fixed in the CH. Finally, the other 5 surfaces were also in situ polymerized on the surfaces of the CH in the same way to form the AGH based sensor that completely encapsulating hydrogel.

General Characterization: Scanning electron microscope (SEM, MAIA3 LMH, from TESCAN, USA) was performed to observe the microstructure of internal hydrogel, where the hydrogel was quenched in nitrogen and vacuum freeze-dried in lyophilizer (JL-A10N-80C, Shanghai, China). The optical metalloscope (Axio Scope A1, from Carl Zeiss, Germany) was utilized to observe the interface of AGH. Fourier transform infrared (FTIR) spectroscopy was conducted on a Nicolet iS50 FTIR spectrometer (from Thermo Fisher Scientific, USA) in the spectral range of 650–4000 cm^{-1}. Differential scanning calorimetry (DSC) experiment was performed from –80–100 °C with a heating velocity of 10 °C min^{-1} under N_2 atmosphere by a DISCOVER DSC250 (from TA Instruments, USA). Thermogravimetric analysis (TGA) was performed by a TGA experiment (STA 449F5, NETZSCH, Germany) in the temperature range from 25 to 800 °C with the scanning rate of 10 °C min^{-1} under N_2 flow. Dynamic light scattering (DLS) analysis was performed by a Zetasizer Nano ZSE (from Malvern, UK). The water contact angle (WCA) and oil contact angle (OCA) were measured by an optical contact angle instrument (DSA100, KRUSS, Germany) with water droplets or paraffin oil of 2 µL. Small-angle X-ray scattering (SAXS) measurements of hydrogel adsorbed by surfactant micelles (to avoid the influence of crystalline materials, MXene was not incorporated into the hydrogel) and AGH were tested on a SAXS point 2.0 instrument (Anton Paar, Austria). The effective scattering range of q was 0.01–5 nm^{-1}, where q is scattering vector, $q=4\pi\sin\theta/\lambda$. (2θ is scattering angle and λ is the diffraction wavelength). The surfactant micelles spacing (d) on hydrogel was calculated by $d=2\pi/q$.

Mechanical Properties Measurement: All mechanical property measurements were performed by a CMT1503 universal mechanical tester (SUST, Zhuhai, China) with a 100 N load cell. The measured sample was prepared into a rectangular shape (50 mm × 20 mm × 5 mm). The testing velocity for each sample was all set as 50 mm min^{-1} at 25 °C. For testing the mechanical properties in solvents, the sample was immersed in solvents for specific time, then it was immediately put out and tested as above. The elastic modulus (E) was defined as the slope of the linear region of the stress-strain (strain of 0–5%). The

toughness (Γ) was calculated by integrating the area of the tensile stress-strain curves, as shown in following equation:

$$\Gamma = \int_{\varepsilon_0}^{\varepsilon_f} \sigma(\varepsilon) \mathrm{d}\varepsilon \quad (1)$$

where ε_0 and ε_f are the initial stretch and fracture stretch, respectively. The hysteresis energy (U_{hys}) was defined as the integrated area of loading-unloading stress-strain curve, which is shown as follow:

$$U_{hys} = \int_{\text{loading}} \sigma \mathrm{d}\varepsilon - \int_{\text{unloading}} \sigma \mathrm{d}\varepsilon \quad (2)$$

Interfacial Toughness Measurement: A classical 90° peeling test was performed to evaluate the interfacial toughness using a CMT1503 universal mechanical tester (SUST, Zhuhai, China) with a 100 N load cell at 25 °C.[22] The prepared sample was shown in Figure S58 (Supporting Information), in which hydrogel was in the lower layer with the dimension of 100 mm in length, 20 mm in width and 3 mm in thickness, the soft solid material was in the upper layer with the dimension of 120 mm in length, 20 mm in width and 2 mm in thickness. A stiff PET film with 100 µm thickness was bonded on the surface of upper layer to avoid excessive elongation during measurement. During peeling the upper layer, the peeling velocity kept constant with 50 mm min^{-1}. When the tested peeling force reached a plateau, the plateau force was determined by averaging the measured steady force and the interfacial toughness was calculated via dividing the plateau force by the width of hydrogel.

Surface Adhesion Measurement: The surface adhesion behavior was tested by a lab-shear test method.[29] Prior to testing, a rectangular AGH (50 mm × 20 mm × 5 mm) was sandwiched by two pieces of substrates to form a adhesion joint, and pressing it with 10 kPa pressure for 10 min. When the substrate was soft, such as skin, a stiff backing (PET film) was covered on the surface of AGH to avoid the deformation of substrates. Then, the two substrates adhered on the AGH were pulled by the CMT1503 universal mechanical tester (SUST, Zhuhai, China) at the velocity of 50 mm min^{-1} at 25 °C. To measure the adhesion strength of AGH underwater, the adhesion joint was entirely constructed underwater and immersed for 30 min. Then, the adhesion joint was put out and measured in the same way as above. The adhesion strength was calculated as the ratio of the maximum force to the adhesion area of the hydrogel.

Assessments of Dehydration Resistance and Swelling Behavior: The AGH (50 mm × 20 mm ×5 mm, where the thickness of exterior ionogel is ≈100 µm) and virgin CH were placed in open environment at 25 °C with 30% relative humidity. Subsequently, their weights were tested at different time, and compared with the initial weight. Similarly, the water retention of AGH under deformation was performed by applying 100% stain to the AGH. The water retention (WR) was calculated by the following equation:

$$\mathrm{WR} = (W - W_0)/W_0 \times 100\% \quad (3)$$

where *W*0 and *W* indicate the initial mass and the mass after dehydration, respectively.

The AGH and CH was immersed in different solvents (water, brine, pH2 aqueous, pH12 aqueous, hexane, dodecane, paraffin oil and ethanol) at 25 °C, and recorded their weight at different time. The swelling ratio (SR) was calculated by:

$$SR = (\mathrm{W} - \mathrm{W}_0)/\mathrm{W}_0 \times 100\% \quad (4)$$

where *W*0 and *W* indicate the initial mass and the mass after immersing in diverse solvents, respectively.

Electrical Performances Measurement: The real-time sensing performances of sensors were evaluated by the relative resistance variation using a digital source meter (Keithley 2450, USA) with the aid of the universal mechanical tester (SUST, Zhuhai, China) at 25 °C. For the human movement signals measurement, the AGH based sensor was adhered on the skin of volunteers and the real-time resistance signals of sensor was recorded during the human movement. Similarly, the resistance of each AGH based sensors was also measured when the sensing matrix constituted by multiple sensors were utilized to monitor the tactile trajectory and facial expressions signals. The relative resistance variation was calculated as following:

$$\Delta R/R_0 = (R - R_0)/R_0 \times 100\% \quad (5)$$

where *R* and *R*0 are the resistance without and with applied strain, respectively. Informed consent was obtained for all participants involved in the experiments testing the applications of the sensors. In addition, these experiments were approved by the Ethics Board of School of Chemical Engineering, Xi'an Jiaotong University, China.

Supporting Information

Supporting Information is available from the Wiley Online Library or from the author.

Acknowledgements

This work was supported by National Natural Science Foundation of China (No. 22178278 and No. 22205174) and the China Postdoctoral Science Foundation (2020M683469). X.H.Z. acknowledges the support from NSERC-Alberta Innovated Advanced Program. B.X. is grateful for the support from the Engineering and Physical Sciences Research Council (EPSRC, UK) grant-EP/N007921.

Conflict Of Interest

The authors declare no conflict of interest.

Data Availability Statement

The data that support the findings of this study are available in the supplementary material of this article.

Keywords

gel hybrids, interface engineering, mechano-sensing, strain sensors, ultra-stretchable

Received: January 31, 2023
Revised: March 4, 2023
Published online:

[1] M. Liu, S. Wang, L. Jiang, *Nat. Rev. Mater.* **2017**, *2*, 17036.
[2] C. E. Semino, *J Dent Res* **2008**, *87*, 606.
[3] S. J. Singer, G. L. Nicolson, *Science* **1972**, *75*, 720.
[4] R. H. Pearson, I. Pascher, *Nature* **1979**, *281*, 499.
[5] K. Kikuchi, S. Shigeta, K. Numayama-Tsuruta, T. Ishikawa, *Int. J. Pharm.* **2020**, *587*, 119708.
[6] H. Yuk, T. Zhang, G. A. Parada, X. Liu, X. Zhao, *Nat. Commun.* **2016**, *7*, 12028.
[7] K. S. Wu, M. M. Stefik, K. P. Ananthapadmanabhan, R. H. Dauskardt, *Biomaterials* **2006**, *27*, 5861.

[8] J. Y. Sun, C. Keplinger, G. M. Whitesides, Z. Suo, *Adv. Mater.* **2014**, *26*, 7608.
[9] X. Liu, T. C. Tang, E. Tham, H. Yuk, S. Lin, T. K. Lu, X. Zhao, *Proc. Natl. Acad. Sci. USA* **2017**, *114*, 2200.
[10] V. Vallem, Y. Sargolzaeiaval, M. Ozturk, Y. C. Lai, M. D. Dickey, *Adv. Mater.* **2021**, *33*, 2004832.
[11] S. H. Kim, S. Jung, I. S. Yoon, C. Lee, Y. Oh, J. M. Hong, *Adv. Mater.* **2018**, *30*, 1800109.
[12] D. Wirthl, R. Pichler, M. Drack, G. Kettlguber, R. Moser, R. Gerstmayr, F. Hartmann, E. Bradt, R. Kaltseis, C. M. Siket, S. E. Schausberger, S. Hild, S. Bauer, M. Kaltenbrunner, *Sci. Adv.* **2017**, *3*, e1700053.
[13] J. Kang, J. Mun, Y. Zheng, M. Koizumi, N. Matsuhisa, H. C. Wu, S. Chen, J. B. H. Tok, G. H. Lee, L. Jin, Z. Bao, *Nat. Nanotechnol.* **2022**, *17*, 1265.
[14] Y. Zhang, R. Xu, W. Zhao, L. Zhang, R. Wang, Z. Ma, W. Sheng, B. Yu, S. Ma, F. Zhou, *Angew. Chem., Int. Ed.* **2022**, *61*, e202209741.
[15] W. Lin, M. Kluzek, N. Iuster, E. Shimoni, N. Kampf, R. Goldberg, J. Klein, *Science* **2020**, *370*, 335.
[16] C. Keplinger, J. Y. Sun, C. C. Foo, P. Rothemund, G. M. Whitesides, Z. Suo, *Science* **2013**, *341*, 984.
[17] L. Dong, A. K. Agarwal, D. J. Beebe, H. Jiang, *Nature* **2006**, *442*, 551.
[18] J. Tang, J. Li, J. J. Vlassak, Z. Suo, *Soft Matter* **2016**, *12*, 1093.
[19] T. Liu, M. Liu, S. Dou, J. Sun, Z. Cong, C. Jiang, C. Du, X. Pu, W. Hu, Z. L. Wang, *ACS Nano* **2018**, *12*, 2818.
[20] J. Liu, S. Lin, X. Liu, Z. Qin, Y. Yang, J. Zang, X. Zhao, *Nat. Commun.* **2020**, *11*, 1071.
[21] K. Jeong, Y. Lee, Y. Kim, H. Mun, K. U. Kyung, S. G. Im, *Chem. Eng. J.* **2022**, *429*, 132250.
[22] H. Yuk, T. Zhang, S. Lin, G. A. Parada, X. Zhao, *Nat. Mater.* **2016**, *15*, 190.
[23] R. Xu, M. Hua, S. Wu, S. Ma, Y. Zhang, L. Zhang, B. Yu, M. Cai, X. He, F. Zhou, *Matter* **2022**, *5*, 634.
[24] J. Yang, R. Bai, B. Chen, Z. Suo, *Adv. Funct. Mater.* **2019**, *30*, 1901693.
[25] Q. Ge, Z. Chen, J. Cheng, B. Zhang, Y. F. Zhang, H. Li, X. He, C. Yuan, J. Liu, S. Magdassi, S. Qu, *Sci. Adv.* **2021**, *7*, eaba4261.
[26] J. Zhang, L. Wang, Y. Xue, I. M. Lei, X. Chen, P. Zhang, C. Cai, X. Liang, Y. Lu, J. Liu, *Adv. Mater.* **2022**, 2209324.
[27] Y. Yu, H. Yuk, G. A. Parada, Y. Wu, X. Liu, C. S. Nabzdyk, K. Youcef-Toumi, J. Zang, X. Zhao, *Adv. Mater.* **2019**, *31*, 1807101.
[28] M. H. Bai, B. Zhao, Z. Y. T. Liu, Z. L. Zheng, X. Wei, L. Li, K. Li, X. Song, J. Z. Xu, Z. M. Li, *Adv. Mater.* **2022**, *34*, 2108848.
[29] Z. Wang, H. Zhou, D. Liu, X. Chen, D. Wang, S. Dai, F. Chen, B. B. Xu, *Adv. Funct. Mater.* **2022**, *32*, 2201396.
[30] C, Yang , C. Suo, *Nat. Rev. Mater.* **2018**, *3*, 125.
[31] A. Abramson, C. T. Chan, Y. Khan, A. Mermin-Bunnell, N. Matsuhisa, R. Fong, R. Shad, W. Hiesinger, P. Mallick, S. S. Gambhir, *Sci. Adv.* **2022**, *8*, eabn6550.
[32] J. Deng, H. Yuk, J. Wu, C. E. Varela, X. Chen, E. T. Roche, C. F. Guo, X. Zhao, *Nat. Mater.* **2021**, *20*, 229.
[33] T. Zhu, C. Jiang, M. Wang, C. Zhu, N. Zhao, J. Xu, *Adv. Funct. Mater.* **2021**, *31*, 2102433.
[34] X. Pu, M. Liu, X. Chen, J. Sun, C. Du, Y. Zhang, J. Zhai, W. Hu, Z. L. Wang, *Sci. Adv.* **2017**, *3*, e1700015.
[35] C. Larson, B. Peele, S. Li, S. Robinson, M. Totaro, L. Beccai, B. Mazzolai, R. Shepherd, *Science* **2016**, *351*, 1071.
[36] Q. Liu, G. Nian, C. Yang, S. Qu, Z. Suo, *Nat. Commun.* **2018**, *9*, 1.
[37] Y. Cao, Y. J. Tan, S. Li, W. W. Lee, H. Guo, Y. Cai, C. Wang, B. C. K. Tee, *Nat. Electron.* **2019**, *2*, 75.
[38] Z. Yu, P. Wu, *Adv. Mater.* **2021**, *33*, 2008479.
[39] K. Schäfer, H. B. Kolli, M. K. Christensen, S. L. Bore, G. Diezemann, J. Gauss, G. Milano, R. Lund, M. Cascella, *Angew. Chem., Int. Ed.* **2020**, *59*, 18591.
[40] J. S. Pedersen, S. U. Egelhaaf, P. Schurtenberger, *J. Phys. Chem.* **1995**, *99*, 1299.
[41] A. Vitale, R. Bongiovanni, B. Ameduri, *Chem. Rev.* **2015**, *115*, 8835.
[42] Y. Zhang, M. Li, B. Qin, L. Chen, Y. Liu, X. Zhang, C. Wang, *Chem. Mater.* **2020**, *32*, 6310.
[43] H. J. Kim, B. Chen, Z. Suo, R. C. Hayward, *Science* **2020**, *367*, 773.
[44] M. A. Haque, T. Kurokawa, G. Kamita, J. P. Gong, *Macromolecules* **2011**, *44*, 8916.
[45] Y. Wang, D. Liang, Z. Suo, K. Jia, *Extreme Mech. Lett.* **2020**, *39*, 100797.
[46] L. Xu, Z. Huang, Z. Deng, Z. Du, T. L. Sun, Z. H. Guo, K. Yue, *Adv. Mater.* **2021**, *33*, 2105306.
[47] H. Wei, Z. Wang, H. Zhang, Y. Huang, Z. Wang, Y. Zhou, B. B. Xu, *Chem. Mater.* **2021**, *33*, 6731.
[48] W. W. Nichols, *Am. J. Hypertens.* **2005**, *18*, 3S.
[49] Y. Yao, L. Hao, L. Xu, Y. Zhang, L. Qi, Y. Sun, B. Yang, F. N. van de Vosse, Y. Yao, *Sci. Rep.* **2017**, *7*, 5864.